Hindawi
Geofluids
Volume 2022, Article ID 3700109, 13 pages
https://doi.org/10.1155/2022/3700109

Research Article

Pressure Performance Analysis of Inclined Well under Multiple-Well Interference in Offshore Heavy Oil Reservoir

Kuiqian Ma, Gongchang Wang, Yue Gao, Meinan Wang, and Jianguo Liu

Bohai Oilfield Research Institute, Tianjin Branch Company, CNOOC Ltd., Tianjin, China 300459

Correspondence should be addressed to Gongchang Wang; wanggch12@cnooc.com.cn

Received 11 April 2022; Revised 22 May 2022; Accepted 6 June 2022; Published 13 July 2022

Academic Editor: Shuyang Liu

Offshore heavy oil reservoirs are developed mainly by inclined wells, and the well distance has been constantly reduced after several well network adjustments. The well test data are often interfered by adjacent wells, resulting in unsatisfactory well test interpretation results, so it is necessary to conduct studies on the multiwell interference well test problem for inclined wells. In this paper, the threshold pressure gradient of heavy oil and the stress sensitive to permeability are considered comprehensively, and a well test model of inclined wells in dual-media reservoirs under multiwell interference is established. The analytical solution in Laplace space is obtained by using Green function and superposition principle. The results show that the typical pressure dynamic curve can be divided into 12 flow regions, and the pressure derivative curve of the central inclined well is upturned and forms multiple "platforms" under the interference of adjacent wells; the adjacent well interference will aggravate the upward of pressure derivative curve; a critical well inclination angle of the inclined well is 40°. When the well inclination angle is greater than 40°, vertical radial flow similar to horizontal wells will appear. The new model is well matched and interpreted in the application of BZ oil field in Bohai Bay, which provides theoretical guidance for multiwell interference test wells in the similar reservoir.

1. Introduction

Currently common well test interpretation methods assume that only one central test well exists in the reservoir. As the field is developed to a later stage, reservoir connectivity becomes more complex, and interference between adjacent wells becomes more pronounced. The test well pressure dynamic curve is often interfered by adjacent wells, causing the late radial flow section to "upturn," which is often treated as a boundary influence in common single-well test models, leading to mishandling of well test data [1–3]. Onur et al. proposed a pressure recovery model including multiproduction well system [4]. Marhaendrajana et al. developed a method to explain the pressure in a multiwell system by considering the "disturbance effect" as a regional pressure drop [5]. Adewole evaluated the connectivity between wells based on the pressure data of test wells under interference [6]. Deng et al. established an interpretation method for pressure recovery under multiple well interference [7]. Cheng et al. used the multiwell interference method to judge the water inflow direction of horizontal wells [8]. Yang et al. developed a novel interference testing model of a multisegment horizontal well (MSHW) to better understand the interference of injection wells when the horizon observation well is open to produce [9]. Kumar et al. established a mathematical interference testing model of the fractured vuggy carbonate reservoirs that then used to test an observation well and two interfering wells in Tarim oilfield [10]. Han et al. presented an integrated approach based on the analysis of tracer and pressure interference data to obtain the degree of interference between fractured horizontal wells in a multiwell pad [11]. Shiqing et al. plotted the type curve of pressure and the pressure derivative of an interference test of wells connected by a large fracture and verified against interference test data [12].

Due to the special characteristics of offshore platforms, inclined wells can adapt to complex geological problems and increase oil seepage area to improve well production and are now widely used in offshore oil fields. Cinco et al. first analyzed and plotted the pressure dynamics of an

inclined well by building an up-and-down closed test well model [13]. Zhang et al. studied the effect of formation heterogeneity on the pressure of inclined wells [14]. Sousa studied the pressure dynamics of inclined wells in homogeneous reservoirs [15]. Li et al. established which belongs to the inclined well in the composite gas reservoir with a conventional internal zone and low-permeability external zone, which comprehensively considered characteristics of stress sensitivity and non-Darcy flow for low-permeability composite gas reservoirs [16].

In summary, there has been no study on the interference of adjacent wells on the pressure dynamic of inclined well. However, as inclined wells are currently the most dominant development method in offshore oil fields, it is important to study an adjacent well interference well test model applicable to inclined wells. In this paper, considering the stress sensitivity to permeability and the threshold pressure gradient of heavy oil, an inclined well test model under multiwell interference in offshore heavy oil reservoirs is established, and the effects of multiple types of sensitive parameters are analyzed. Finally, the model is well applied in the SZ oil field of Bohai Bay.

2. Model Development

2.1. Nonlinear Seepage of Heavy Oil. Heavy oil has high viscosity, large seepage resistance, and large interaction force between liquid-solid interface and liquid-liquid interface [17–19]. Therefore, the seepage characteristics in porous media are different from those of conventional thin oil and generally show nonlinear seepage characteristics (threshold pressure gradient) [20–23]. Only when the displacement pressure gradient exceeds the threshold pressure gradient does the heavy oil begin to flow, and its seepage characteristics are shown in Figure 1.

The core displacement experiments in Bohai SZ oilfield show that the threshold pressure gradient and mobility of heavy oil in porous media conform to the nonlinear relationship, as shown in Figure 2. When the mobility is small, the pressure gradient decreases rapidly with the increase of mobility. With the continuous increase of mobility, the decline of threshold pressure gradient slows down and is matched by exponential function, as shown in Equation (1). The reason for this phenomenon is that with the decrease of viscosity of heavy oil, the content of gum, asphaltene, and high molecular hydrocarbons in heavy oil decreases, resulting in the weakening of structural characteristics of heavy oil, the reduction of intermolecular force during flow, and the reduction of flow resistance. With the increase of permeability, the faster the resistance decreases,

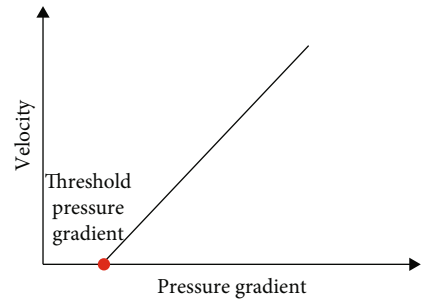

Figure 1: Heavy oil seepage characteristics dynamic curve.

resulting in the gradual decrease of heavy oil threshold pressure gradient with the increase of mobility.

$$\lambda_B = a\left(\frac{K}{\mu_o}\right)^{-b}. \tag{1}$$

2.2. Physical Model. As is shown in Figure 3, there is a central test inclined well in infinite outer boundary reservoir, and the surrounding adjacent wells have good connectivity with it:

(1) The Warren-Root model is adopted to describe the dual-porosity formation

(2) The interporosity flow is calculated through the pseudo-steady-state model

(3) Stress sensitivity of permeability is considered

(4) Heavy oil in porous media has the property of threshold pressure gradient

2.3. Mathematical Model. Considering the permeability stress-sensitive of reservoir and the threshold pressure gradient of heavy oil fluid, the fluid motion equation is improved as follows:

$$v_{fr} = \frac{K_{fh}}{\mu} e^{-\gamma(p_i - p_f)}\left(\frac{\partial p_f}{\partial r} - \lambda_B\right), \tag{2}$$

$$v_{fz} = \frac{K_{fv}}{\mu} e^{-\gamma(p_i - p_f)}\left(\frac{\partial p_f}{\partial r} - \lambda_B\right). \tag{3}$$

By virtue of Equation (1) and Equation (2), the seepage differential equation of central test inclined well describing the threshold pressure gradient of heavy oil in stress sensitive reservoir is obtained:

$$\begin{cases} \dfrac{K_{fh}}{\mu}\dfrac{1}{r}\dfrac{\partial}{\partial r}\left[re^{-\gamma(p_i-p_f)}\left(\dfrac{\partial p_f}{\partial r} - \lambda_B\right)\right] + \dfrac{K_{fv}}{\mu}\dfrac{\partial}{\partial z}\left[e^{-\gamma(p_i-p_f)}\left(\dfrac{\partial p_f}{\partial z} - \lambda_B\right)\right] = (\phi C_t V)_f \dfrac{\partial p_f}{\partial t} - \dfrac{\alpha K_m}{\mu}(p_m - p_f), \\ (\phi C_t V)_m \dfrac{\partial p_m}{\partial t} + \dfrac{\alpha K_m}{\mu}(p_m - p_f) = 0. \end{cases} \tag{4}$$

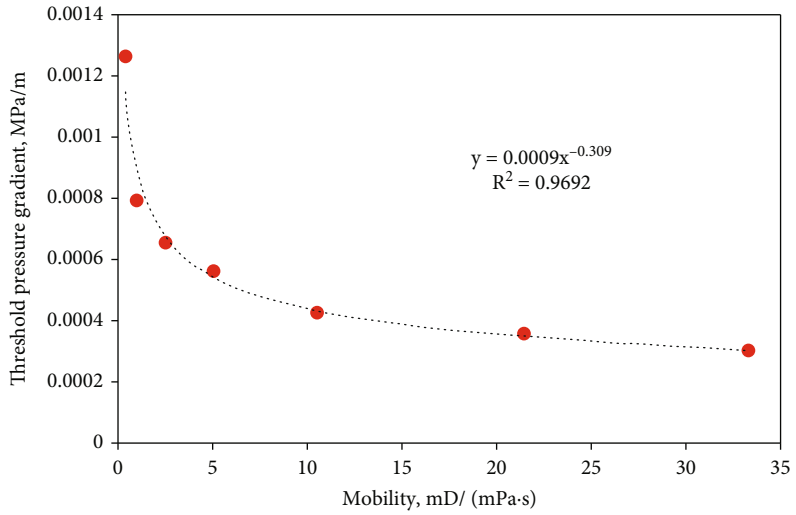

Figure 2: Relation curve between pressure gradient and mobility.

The following is the differential equation of adjacent interference wells:

$$\begin{cases} \dfrac{K_{\mathrm{fh}}}{\mu}\dfrac{1}{r}\dfrac{\partial}{\partial r}\left[re^{-\gamma(p_{\mathrm{i}}-p_{\mathrm{f}})}\left(\dfrac{\partial p_{\mathrm{f}}}{\partial r}-\lambda_{\mathrm{B}}\right)\right]=(\phi C_{\mathrm{t}}V)_{\mathrm{f}}\dfrac{\partial p_{\mathrm{f}}}{\partial t}-\dfrac{\alpha K_{\mathrm{m}}}{\mu}(p_{\mathrm{m}}-p_{\mathrm{f}}), \\ (\phi C_{\mathrm{t}}V)_{\mathrm{m}}\dfrac{\partial p_{\mathrm{m}}}{\partial t}+\dfrac{\alpha K_{\mathrm{m}}}{\mu}(p_{\mathrm{m}}-p_{\mathrm{f}})=0. \end{cases} \tag{5}$$

Since the values of $(\partial p_{\mathrm{f}}/\partial r)\times\lambda_{\mathrm{B}}$ and $(\partial p_{\mathrm{f}}/\partial z)\times\lambda_{\mathrm{B}}$ are small, they can be rounded off and the above equation can be simplified as follows.

Central test inclined well:

$$\begin{cases} K_{\mathrm{fh}}\left[\dfrac{1}{r}\dfrac{\partial}{\partial r}\left(r\dfrac{\partial p_{\mathrm{f}}}{\partial r}\right)+\gamma\left(\dfrac{\partial p_{\mathrm{f}}}{\partial r}\right)^{2}-\dfrac{\lambda_{\mathrm{B}}}{r}\right]+K_{\mathrm{fv}}\left[\dfrac{\partial^{2}p_{\mathrm{f}}}{\partial z^{2}}+\gamma\left(\dfrac{\partial p_{\mathrm{f}}}{\partial z}\right)^{2}\right]=e^{\gamma(p_{i}-p_{\mathrm{f}})}\left[(\phi C_{\mathrm{t}}V)_{\mathrm{f}}\mu\dfrac{\partial p_{\mathrm{f}}}{\partial t}-\alpha K_{\mathrm{m}}(p_{\mathrm{m}}-p_{\mathrm{f}})\right], \\ (\phi C_{\mathrm{t}}V)_{\mathrm{m}}\dfrac{\partial p_{\mathrm{m}}}{\partial t}+\dfrac{\alpha K_{\mathrm{m}}}{\mu}(p_{\mathrm{m}}-p_{\mathrm{f}})=0. \end{cases} \tag{6}$$

Adjacent interference well:

$$\begin{cases} K_{\mathrm{fh}}\left[\dfrac{1}{r}\dfrac{\partial}{\partial r}\left(r\dfrac{\partial p_{\mathrm{f}}}{\partial r}\right)+\gamma\left(\dfrac{\partial p_{\mathrm{f}}}{\partial r}\right)^{2}-\dfrac{\lambda_{\mathrm{B}}}{r}\right]=e^{\gamma(p_{\mathrm{i}}-p_{\mathrm{f}})}\left[(\phi C_{\mathrm{t}}V)_{\mathrm{f}}\mu\dfrac{\partial p_{\mathrm{f}}}{\partial t}-\alpha K_{\mathrm{m}}(p_{\mathrm{m}}-p_{\mathrm{f}})\right], \\ (\phi C_{\mathrm{t}}V)_{\mathrm{m}}\dfrac{\partial p_{\mathrm{m}}}{\partial t}+\dfrac{\alpha K_{\mathrm{m}}}{\mu}(p_{\mathrm{m}}-p_{\mathrm{f}})=0. \end{cases} \tag{7}$$

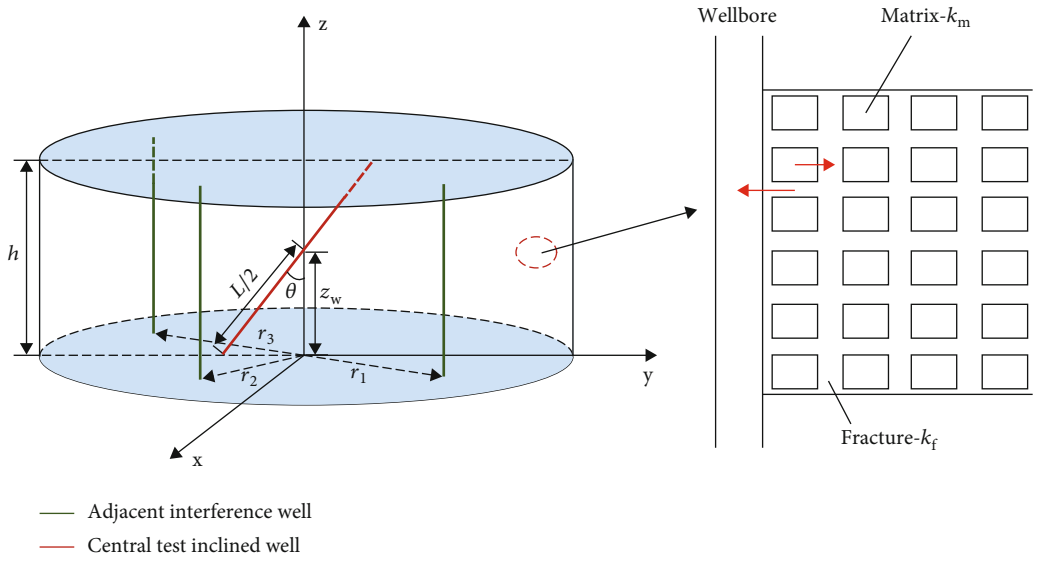

Figure 3: Physical model diagram.

Dimensionless quantities are defined as follows:

$p_{fD} = (2\pi\ K_{fh}h/q\mu)\ (p_i - p_f)\ p_{mD} = (2\pi K_m\ h/q\mu)(p_i - p_m)\ t_D = (K_{fh}t/\mu r_w^2(V\phi C_t)_{f+m})\omega = ((V\phi\ C_t)_f/(V\phi C_t)_{f+m})\lambda_m = \alpha r_w^2\ (K_m/K_{fh})\gamma_D = (q\mu B/K_{fh}h)\gamma\lambda_{BD} = (K_{fh}hr_w/q\mu B)\ \lambda_B\ r_D = (r/r_w)\ z_D = (z/h)C_D = (C/(V\phi C_t)_{f+m}hr\ w^2)L_D = (L/h)\sqrt{K_{fh}/K_{fv}}\ h_D = (h/r_w)\ \sqrt{K_{fh}/K_{fv}}$.

Substituting the above dimensionless quantities into formulas (5) and (6), the dimensionless seepage differential equation is obtained:

$$\begin{cases} \dfrac{1}{r_D}\dfrac{\partial}{\partial r_D}\left(r_D\dfrac{\partial p_{fD}}{\partial r_D}\right) - \gamma_D\left(\dfrac{\partial p_{fD}}{\partial r_D}\right) + \dfrac{\lambda_{BD}}{r_D} + \left[\dfrac{\partial^2 p_{fD}}{\partial z_D^2} + \gamma_D\left(\dfrac{\partial p_{fD}}{\partial z_D}\right)^2\right] = e^{\gamma_D p_{fD}}\left[\omega\dfrac{\partial p_{fD}}{\partial t_D} - \lambda_m(p_{mD} - p_{fD})\right], \\ \omega\dfrac{\partial p_{mD}}{\partial t_D} + \lambda_m(p_{mD} - p_{fD}) = 0, \end{cases} \tag{8}$$

$$\begin{cases} \dfrac{1}{r_{jD}}\dfrac{\partial}{\partial r_{jD}}\left(r_{jD}\dfrac{\partial p_{fD}}{\partial r_{jD}}\right) - \gamma_D\left(\dfrac{\partial p_{fD}}{\partial r_{jD}}\right) + \dfrac{\lambda_{BD}}{r_{jD}} = e^{\gamma_D p_{fD}}\left[\omega\dfrac{\partial p_{fD}}{\partial t_{jD}} - \lambda_m(p_{mD} - p_{fD})\right], \\ \omega\dfrac{\partial p_{mD}}{\partial t_{jD}} + \lambda_m(p_{mD} - p_{fD}) = 0. \end{cases} \tag{9}$$

Central test inclined well is as follows:

Initial condition

$$p_{fD}(r_D, 0) = p_{mD}(r_D, 0) = 0. \tag{10}$$

Outer boundary condition

$$p_{fD}\big|_{r_D\longrightarrow\infty} = p_{mD}\big|_{r_D\longrightarrow\infty} = 0. \tag{11}$$

Inner boundary condition

$$\lim_{\varepsilon\longrightarrow 0}\left[\lim_{r_D\longrightarrow 0}\int_{z_{wD}-\varepsilon/2}^{z_{wD}+(\varepsilon/2)} r_D e^{-\gamma_D p_{fD}}\left(\frac{\partial p_{fD}}{\partial r_D} + \lambda_{BD}\right)dz_D\right] = -h_D\,|z_D - z_{wD}| \le \frac{\varepsilon}{2}. \tag{12}$$

Adjacent interference well ($j = 1, 2, 3 \cdots$) is as follows.
Initial condition

$$p_{\mathrm{fD}}\left(r_{\mathrm{jD}}, 0\right) = p_{\mathrm{mD}}\left(r_{\mathrm{jD}}, 0\right) = 0. \tag{13}$$

Outer boundary condition

$$p_{\mathrm{fD}}\Big|_{r_{\mathrm{jD}}\longrightarrow\infty} = p_{\mathrm{mD}}\Big|_{r_{\mathrm{jD}}\longrightarrow\infty} = 0. \tag{14}$$

Inner boundary condition

$$r_{\mathrm{jD}}\frac{\partial p_{\mathrm{fD}}}{\partial r_{\mathrm{jD}}}\Big|_{r_{\mathrm{jD}}=1} - \lambda_{\mathrm{BD}} = -q_{\mathrm{jD}}. \tag{15}$$

Top and bottom conditions for

$$\frac{\partial p_{\mathrm{fD}}}{\partial z_{\mathrm{D}}}\Big|_{z_{\mathrm{D}}=0} = \frac{\partial p_{\mathrm{mD}}}{\partial z_{\mathrm{D}}}\Big|_{z_{\mathrm{D}}=0} = 0, \tag{16}$$

$$\frac{\partial p_{\mathrm{fD}}}{\partial z_{\mathrm{D}}}\Big|_{z_{\mathrm{D}}=h_{\mathrm{D}}} = \frac{\partial p_{\mathrm{mD}}}{\partial z_{\mathrm{D}}}\Big|_{z_{\mathrm{D}}=h_{\mathrm{D}}} = 0. \tag{17}$$

3. Model Solution

In order to eliminate the quadratic term in the above dimensionless equation, Pedrosa variable substitution and regular perturbation method are used:

$$p_{\mathrm{fD}} = -\frac{1}{\gamma_{\mathrm{D}}}\ln\left(1 - \gamma_{\mathrm{D}}\xi_{\mathrm{D}}\right). \tag{18}$$

Because $\gamma_{\mathrm{D}} \ll 1$, the zero order perturbation solution is taken, and then, Laplace transform is performed on it. Finally, equations (5) and (6) become as follows:

Central test inclined well:

$$\frac{1}{r_{\mathrm{D}}}\frac{\partial}{\partial r_{\mathrm{D}}}\left(r_{\mathrm{D}}\frac{\partial \bar{\xi}_{\mathrm{D0}}}{\partial r_{\mathrm{D}}}\right) + \frac{\lambda_{\mathrm{BD}}}{s r_{\mathrm{D}}} + \frac{\partial^2 \bar{\xi}_{\mathrm{D0}}}{\partial z_{\mathrm{D}}^2} = \omega s\bar{\xi}_{\mathrm{D0}} + (1-\omega)s\bar{p}_{\mathrm{mD}}, \tag{19}$$

$$\bar{p}_{\mathrm{mD}} = \frac{\lambda_{\mathrm{m}}}{\lambda_{\mathrm{m}} + (1-\omega)s}\bar{\xi}_{\mathrm{D0}}, \tag{20}$$

$$\bar{\xi}_{\mathrm{D0}}\big|_{r_{\mathrm{D}}\longrightarrow\infty} = \bar{p}_{\mathrm{mD}}\big|_{r_{\mathrm{D}}\longrightarrow\infty} = 0, \tag{21}$$

$$\lim_{\varepsilon\longrightarrow 0}\left[\lim_{r_{\mathrm{D}}\longrightarrow 0}\int_{z_{\mathrm{wD}}-\varepsilon/2}^{z_{\mathrm{wD}}+(\varepsilon/2)} r_{\mathrm{D}}e^{-\gamma_{\mathrm{D}}p_{\mathrm{fD}}}\left(\frac{\partial \bar{\xi}_{\mathrm{D0}}}{\partial r_{\mathrm{D}}} + \lambda_{\mathrm{BD}}\right)dz_{\mathrm{D}}\right] = -h_{\mathrm{D}}, \left|z_{\mathrm{D}} - z_{\mathrm{wD}}\right| \le \frac{\varepsilon}{2}. \tag{22}$$

Adjacent interference well ($j = 1, 2, 3 \cdots$):

$$\frac{1}{r_{\mathrm{jD}}}\frac{\partial}{\partial r_{\mathrm{jD}}}\left(r_{\mathrm{jD}}\frac{\partial \bar{\xi}_{\mathrm{D0j}}}{\partial r_{\mathrm{jD}}}\right) + \frac{\lambda_{\mathrm{BD}}}{s r_{\mathrm{D}}} = \omega s\bar{\xi}_{\mathrm{D0j}} + (1-\omega)s\bar{p}_{\mathrm{mD}}, \tag{23}$$

$$\bar{p}_{\mathrm{mD}} = \frac{\lambda_{\mathrm{m}}}{\lambda_{\mathrm{m}} + (1-\omega)s}\bar{\xi}_{\mathrm{D0j}}, \tag{24}$$

$$\bar{\xi}_{\mathrm{D0j}}\Big|_{r_{\mathrm{jD}}\longrightarrow\infty} = \bar{p}_{\mathrm{mD}}\Big|_{r_{\mathrm{jD}}\longrightarrow\infty} = 0, \tag{25}$$

$$\frac{\partial \bar{\xi}_{\mathrm{D0j}}}{\partial r_{\mathrm{jD}}} + \frac{\lambda_{\mathrm{BD}}}{s} = -\frac{q_{\mathrm{jD}}}{s}, \tag{26}$$

$$\frac{\partial \bar{\xi}_{\mathrm{D0}}}{\partial z_{\mathrm{D}}}\Big|_{z_{\mathrm{D}}=0} = \frac{\partial p_{\mathrm{mD}}}{\partial z_{\mathrm{D}}}\Big|_{z_{\mathrm{D}}=0} = 0, \tag{27}$$

$$\frac{\partial \bar{\xi}_{\mathrm{D0}}}{\partial z_{\mathrm{D}}}\Big|_{z_{\mathrm{D}}=h_{\mathrm{D}}} = \frac{\partial p_{\mathrm{mD}}}{\partial z_{\mathrm{D}}}\Big|_{z_{\mathrm{D}}=h_{\mathrm{D}}} = 0. \tag{28}$$

According to the superposition principle, the finite cosine integral transform of the model under Laplace space with respect to z_{D}, and then using the Green function and the zero-order regenerative solution, the point source solution of the model can be found as

$$\begin{aligned}\bar{\xi}_{\mathrm{D}} \approx \bar{\xi}_{\mathrm{D0}} + \bar{\xi}_{\mathrm{D0j}} &= \frac{1}{s}K_0\left[r_{\mathrm{D}}\sqrt{sf(s)}\right] \\ &+ \frac{2}{s}\sum_{n=1}^{\infty}K_0\left(r_{\mathrm{D}}\sqrt{sf(s) + \frac{n^2\pi^2}{h_{\mathrm{D}}^2}}\right)\times\cos\left(\frac{n\pi z_{\mathrm{D}}}{h_{\mathrm{D}}}\right)\cos\left(\frac{n\pi z_{\mathrm{wD}}}{h_{\mathrm{D}}}\right) \\ &+ \sum_{\mathrm{j}=1}^{m}\left[\frac{q_{\mathrm{Dj}}\mathrm{K}_0\left(r_{\mathrm{jD}}\sqrt{sf(s)}\right)}{s\sqrt{sf(s)}\mathrm{K}_1\left(\sqrt{sf(s)}\right)} + \int_0^{+\infty}G\left(r_{\mathrm{jD}}, \tau\right)d\tau\right] \\ &+ \int_0^{+\infty}G(r_{\mathrm{D}}, \tau)d\tau.\end{aligned} \tag{29}$$

Assuming that the flow in the wellbore of the central inclined well is evenly inferenced, according to the point source theory, the point source solution is integrated along the wellbore direction, and the bottom hole pressure solution of the central inclined well under multiwell interference can be obtained.

$$\begin{aligned}\bar{\xi}_{\mathrm{wDN}} &= \frac{1}{sL_{\mathrm{D}}}\int_{-L_{\mathrm{D}}/2}^{L_{\mathrm{D}}/2}K_0[\bar{r}_{\mathrm{D}}sf(s)]d\eta \\ &+ \frac{2}{sL_{\mathrm{D}}}\int_{-L_{\mathrm{D}}/2}^{L_{\mathrm{D}}/2}\sum_{n=1}^{\infty}K_0\left(\bar{r}_{\mathrm{D}}\sqrt{sf(s) + \frac{n^2\pi^2}{h_{\mathrm{D}}^2}}\right) \\ &\times\cos\left(\frac{n\pi z_{\mathrm{D}}}{h_{\mathrm{D}}}\right)\cos\left(\frac{n\pi\bar{z}_{\mathrm{wD}}}{h_{\mathrm{D}}}\right)d\eta + \frac{1}{L_{\mathrm{D}}}\int_0^{+\infty}\int_{-L_{\mathrm{D}}/2}^{L_{\mathrm{D}}/2}G(\bar{r}_{\mathrm{D}}, \tau)d\eta d\tau \\ &+ \sum_{\mathrm{j}=1}^{m}\left[\frac{q_{\mathrm{Dj}}\mathrm{K}_0\left(r_{\mathrm{jD}}\sqrt{sf(s)}\right)}{s\sqrt{sf(s)}\mathrm{K}_1\left(\sqrt{sf(s)}\right)} + \int_0^{+\infty}G\left(r_{\mathrm{jD}}, \tau\right)d\tau\right],\end{aligned} \tag{30}$$

$$\bar{r}_{\mathrm{D}} = \sqrt{\left(x_{\mathrm{D}} - x_{\mathrm{wD}} - \eta\sin\theta_{\mathrm{w}}\right)^2 + \left(y_{\mathrm{D}} - y_{\mathrm{wD}}\right)^2}, \tag{31}$$

$$\bar{z}_{\mathrm{wD}} = z_{\mathrm{wD}} + \eta\cos\theta_{\mathrm{w}}, \tag{32}$$

$$\theta_w = \arctan\left(\sqrt{\frac{K_{fv}}{K_{fh}}}\tan\theta\right), \tag{33}$$

$$L_D = \frac{L}{r_w}\sqrt{\frac{K_{fv}}{K_{fh}}\sin^2\theta + \frac{K_{fv}}{K_{fh}}\cos^2\theta}. \tag{34}$$

Duhamel principle and pressure drop superposition principle are used to solve the bottom hole pressure solution of the central inclined well under the interference of multi-wells.

$$\bar{\xi}_{WD} = \frac{s\bar{\xi}_{WDN} + S}{s + C_D s^2\left(s\bar{\xi}_{WDN} + S\right)}. \tag{35}$$

Through Stehfest numerical inversion, the bottom hole pressure solution in real space can be obtained [24, 25]:

$$p_{wD} = -\frac{1}{\gamma_D}\ln\left(1 - \gamma_D\bar{\xi}_{WD}\right). \tag{36}$$

4. Results and Discussion

4.1. Model Verification. When dimensionless threshold pressure gradient (λ_{BD}), dimensionless stress sensitivity coefficients (γ_D), and well inclination angle (θ) are taken as zero, as well there is no interference from adjacent wells, the model is the same as the conventional vertical well pressure drawdown well test model of dual media reservoir. In order to verify the model in the paper, the type curve obtained by the numerical method is compared with the conventional dual media reservoir well test curve obtained by the analytical solution shown in Figure 4.

As shown in Figure 4, the type curve of pressure drawdown well test obtained by the numerical solution and the analytical solution are the same when dimensionless threshold pressure gradient (λ_{BD}), dimensionless stress sensitivity coefficients (γ_D), and well inclination angle (θ) are taken as zero, as well there is no interference from adjacent wells. Thus, the numerical solution in the paper is reliable.

4.2. Type Curves. The pressure solution in real space is obtained by numerical inversion. Taking the existence of three adjacent wells around the central inclined well as an example, its pressure curve and pressure derivative curve are plotted as shown in Figures 5–12; flow regions are identified.

Region 1. The early wellbore storage period: the pressure curve and pressure derivative curve are line segments with a slope equal to "1," reflecting the effect of wellbore reservoir effects

Region 2. The skin effect period: the major influential factor in this period is the skin factor effect, and the pressure derivative curve presents the shape of "hump"

Region 3. Well inclination angle influence period: the pressure derivative curve presents the shape of "concavity," which reflects the influence of well inclination angle. When the well inclination angle is large, it shows the characteristics of vertical radial flow in horizontal wells; when the well inclination angle is small, it shows the characteristics of radial flow for vertical wells

Region 4. Fracture radial flow period: the major influential factor in this period is the flow of fluid from fracture to bottom hole, and the pressure derivative curve is a straight horizontal line

Region 5. Leakage period: the major influential factor in this period is the leakage capacity of matrix to fracture, and the pressure derivative curve presents the shape of "concavity"

Region 6. First radial flow period: the major influential factor in this period is the late radial flow of the central inclined well, and the pressure derivative curve is a straight horizontal line

Region 7. Transitional flow period: transition period between radial flows

Region 8. Second radial flow period: it reflects the radial flow characteristics of the central inclined well interfered by the nearest adjacent well, and the pressure derivative curve is a straight horizontal line

Region 9. Transitional flow period: transition period between radial flows

Region 10. Third radial flow period: it reflects the radial flow characteristics of the central inclined well interfered by the two nearest adjacent well, and the pressure derivative curve is a straight horizontal line

Region 11. Transitional flow period: transition period between radial flows

Region 12. Fourth radial flow period: it reflects the radial flow characteristics of the central inclined well interfered by the three nearest adjacent well, and the pressure derivative curve is a straight horizontal line

4.3. Sensitivity Analysis

4.3.1. Permeability Modulus. As shown in Figure 6, with the increase of permeability modulus, the pressure dynamic curve is gradually upward after region 7, and the larger the permeability modulus is, the greater the degree of upward. The reason for the above phenomenon is that the larger the permeability modulus is, the greater the decrease of permeability with the increase of pressure; therefore, the resistance of fluid flow becomes larger and the pressure required for flow is also larger. When the permeability modulus is large, the reservoir permeability decreases sharply under higher pressure in the late stage of seepage, and the pressure dynamic curve reflects a characteristic similar to a closed outer boundary.

4.3.2. Threshold Pressure Gradient. As shown in Figure 7, the higher the threshold pressure gradient of heavy oil, the greater the upward warping degree of pressure dynamic curve, and the upward warping is obvious after region 7. This is because heavy oil has threshold pressure gradient, the flow capacity of heavy oil in pores is weakened, and the displacement pressure difference required for heavy oil flow is also larger.

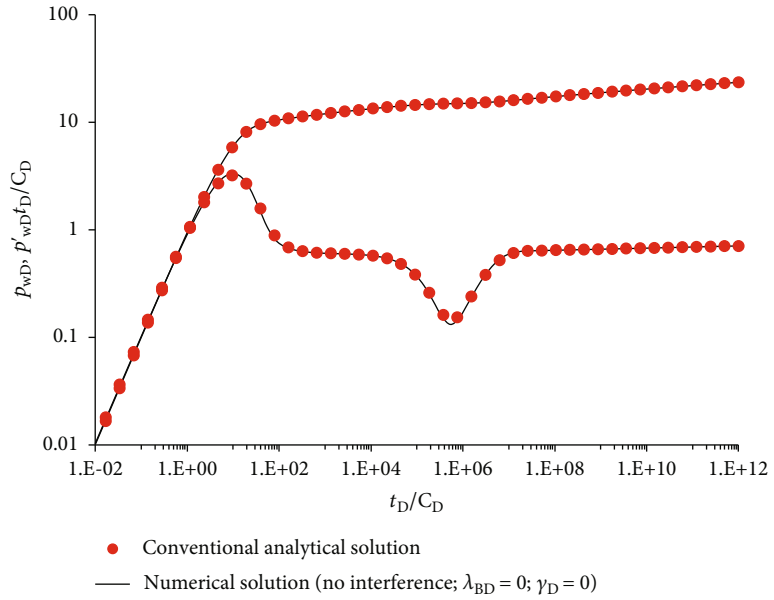

FIGURE 4: Comparison between the numerical solution and the analytical solution to the pressure drawdown well test.

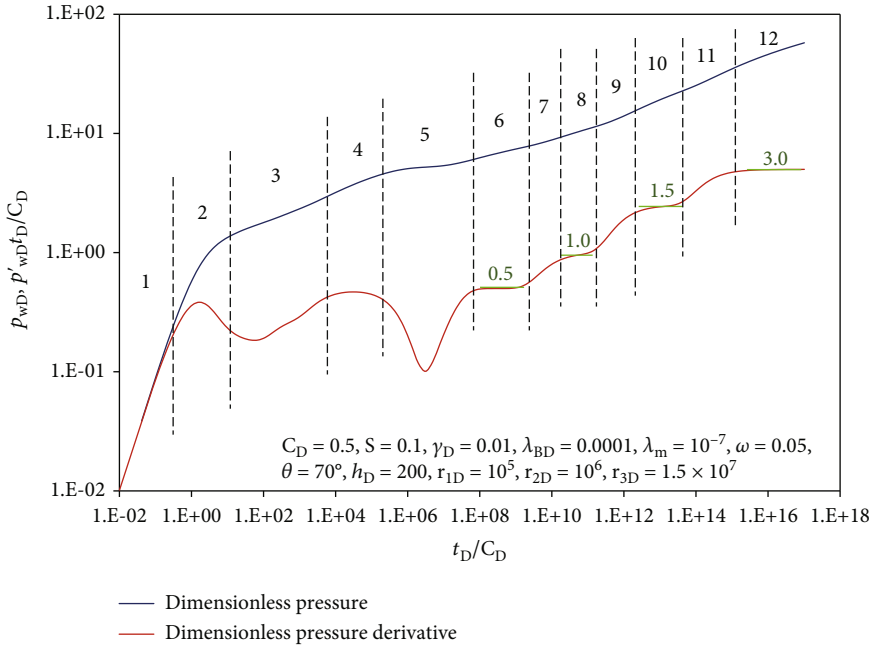

FIGURE 5: Typical pressure dynamic curves.

4.3.3. Production of Adjacent Wells. As shown in Figure 8, taking the example of the presence of three connected adjacent wells around the central inclined well, the pressure dynamic profile of the central inclined well has four late radial flow stages and the ratio of the N^{th} ($N > 2$) radial flow value to the first radial flow value is equal to $1 + \sum_{j=1}^{k} q_{jD}$ (k is the number of adjacent wells that have an influence on the N^{th} radial flow stage). Taking $q_{1D} = q_{2D} = q_{3D} = 1$ as an example, the third radial flow stage is the result of the joint influence of the test well and the two adjacent wells, so the value of the third radial flow is $0.5 * (1 + 2) = 1.5$.

4.3.4. Well Inclination Angle. As shown in Figure 9, the greater the well inclination angle, the greater the wellbore pressure drop and the lower the pressure dynamic curve. Because the inclined well completely penetrates the formation, the larger well inclination angle is, the longer the wellbore length is. Under the assumption of equal flow in the wellbore, the longer the wellbore length L, the greater the pressure drop in the wellbore. And the well inclination angle mainly affects the flow near the well, when well inclination angle is large ($\theta > 40°$), the curve will show an early vertical radial flow similar to that of a horizontal well, and when

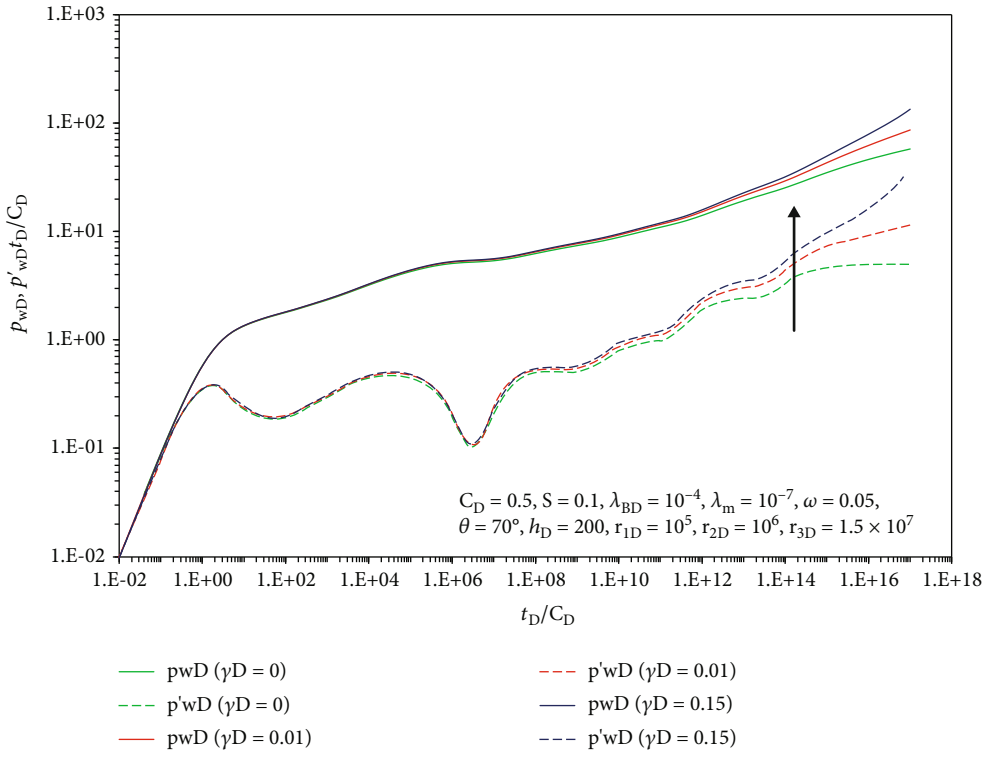

Figure 6: Influence of permeability modulus on pressure dynamic curve.

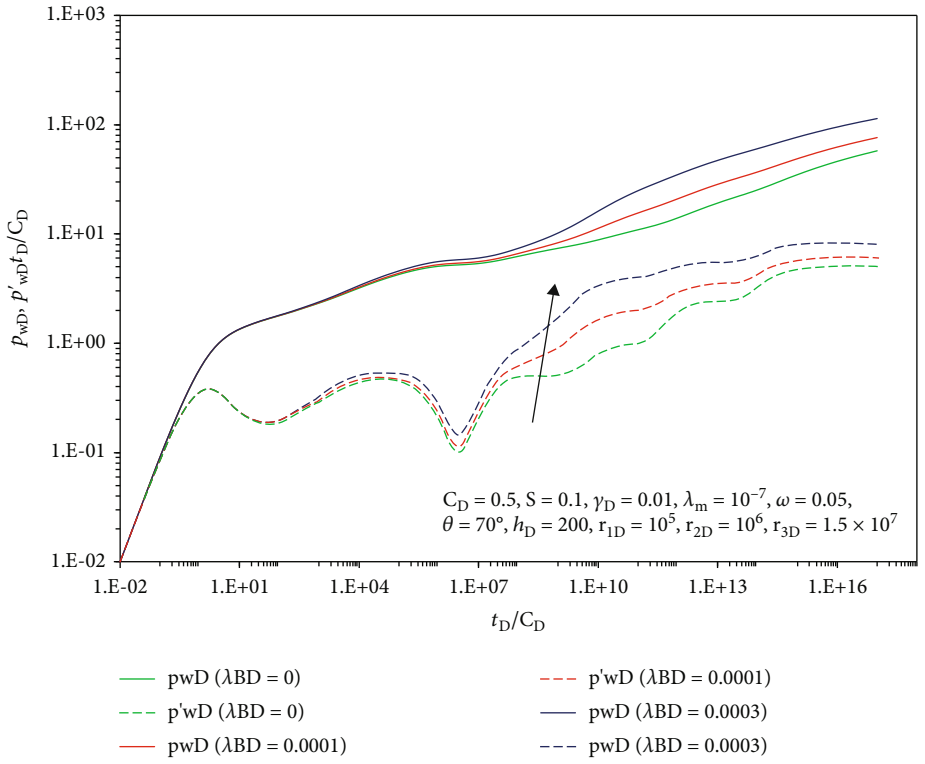

Figure 7: Influence of threshold pressure gradient on pressure dynamic curve.

the well inclination angle is relatively small ($\theta < 40^\circ$), the characteristics of vertical radial flow disappear, which is similar to the radial flow of vertical wells.

4.3.5. Adjacent Well Distance. As shown in Figure 10, as the distance between the adjacent well and the central inclined well increases, the start time of the second radial flow is

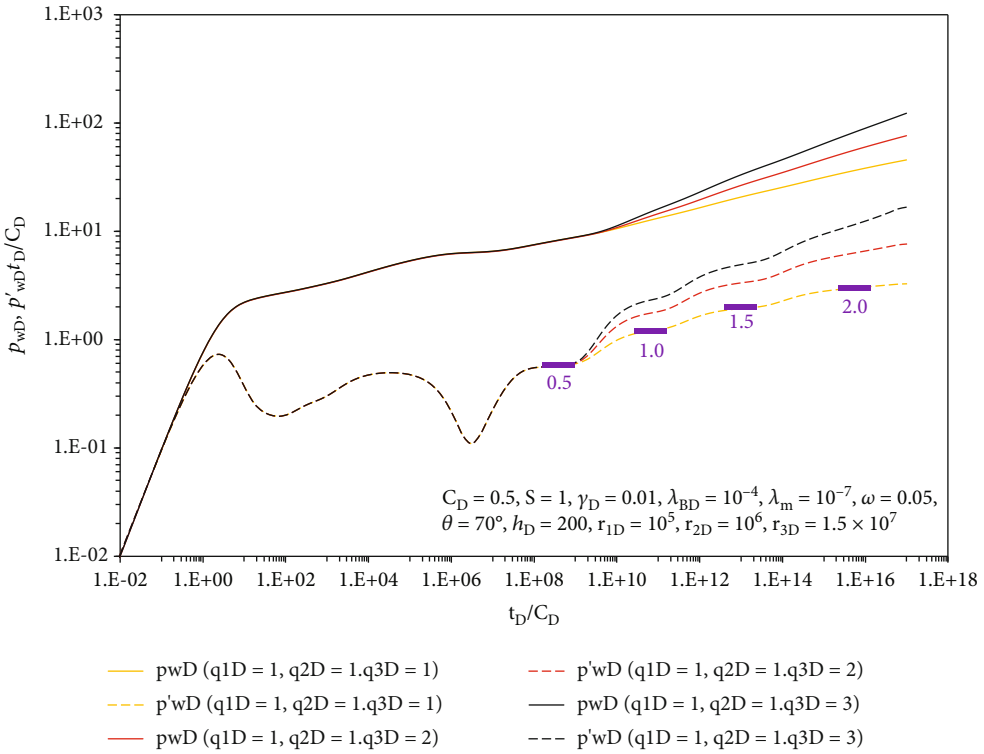

Figure 8: Influence of production of adjacent wells on pressure dynamic curve.

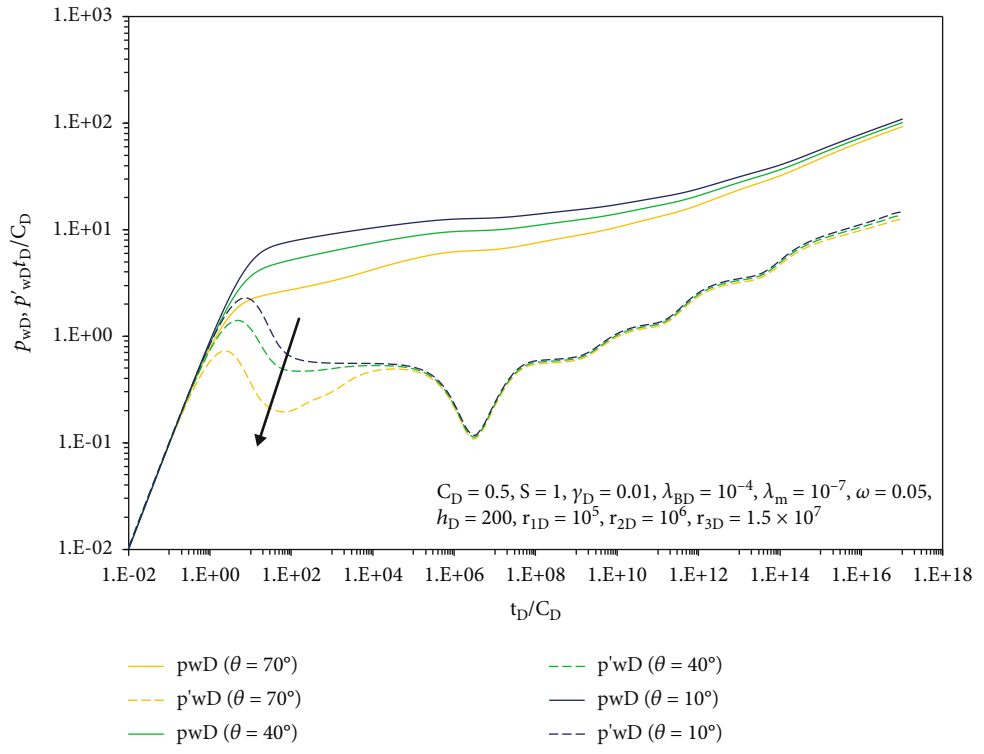

Figure 9: Influence of well inclination angle on pressure dynamic curve.

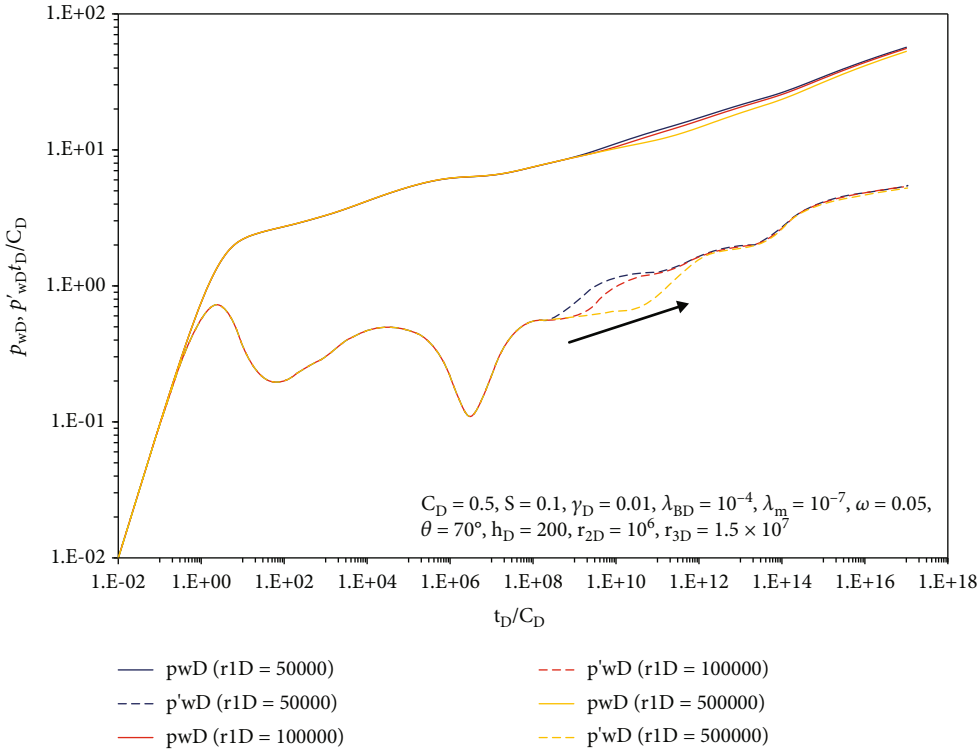

Figure 10: Influence of distance on pressure dynamic curve.

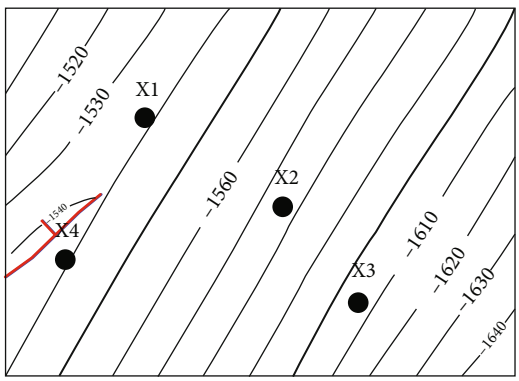

Figure 11: Well location diagram.

delayed and the shift duration becomes shorter. When the distance is short, the second radial flow section gradually disappears and integrates into the third radial flow section.

5. Field Application

5.1. Field Test Data Matching Method. In order to reduce the nonuniqueness, the following steps should be followed when applying the model to well test interpretation of field test data:

(1) Using the actual pressure recovery data, draw the pressure curve and pressure derivative curve. Judging whether there are multiple radial flow period in the later stage of the pressure response curve, if it conforms to the interference well test curve of adjacent wells, the adjacent well interference model is used for parameter interpretation; otherwise, the ordinary single well model is adopted

(2) According to the selected well test interpretation model (without considering the influence of stress sensitivity and threshold pressure gradient), the initial pressure response curve is matched by changing wellbore storage coefficient, skin coefficient, interporosity flow coefficient, and elastic storativity ratio

(3) Input the distance between adjacent wells and the production of adjacent wells to match the multistage radial flow section in the later stage

(4) The interpretation result parameters of adjacent wells in conventional reservoir are taken as the initial parameters and input into the interference well test model of adjacent wells in dual media reservoir considering stress sensitivity and threshold pressure gradient. The pressure response curve is further matched and interpreted by changing the stress sensitivity coefficient and start-up pressure gradient. Finally, the relevant parameters are obtained

5.2. Example Explanation. SZ reservoir is located in Bohai Bay, China. It is a heavy oil reservoir with an average oil viscosity of 320 mPa·s. X2 well is an inclined well in SZ reservoir, with an inclination angle of 73°, and effective thickness of the reservoir is 31.5 m, porosity of 13.5%, and volume coefficient of 1.06. Through the reservoir sand

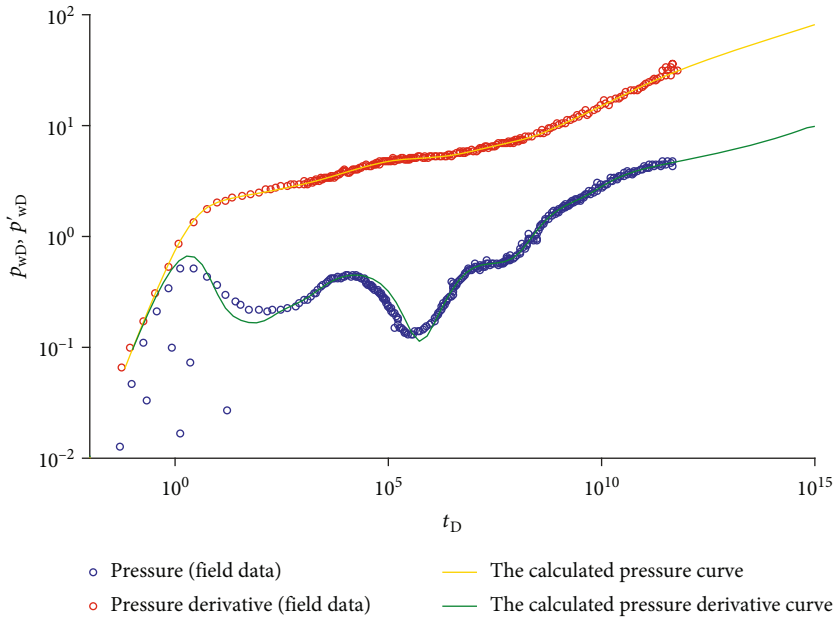

Figure 12: Pressure matching curve.

Table 1: The basic parameters for the investigated reservoir.

Well name	Distance (m)	Daily liquid production (m^3/d)
X1	173	200
X3	162	150
X4	218	200

Table 2: The interpretation results.

Parameters	Value
Wellbore storage coefficient	0.17 m^3/MPa
Skin factor	0.09
Interporosity flow coefficient	5.7×10^{-7}
Permeability	1420 mD
Storativity ratio	5.4×10^{-2}
Threshold pressure gradient	2.4×10^{-4} MPa/m
Permeability modulus	1.5×10^{-2} MPa^{-1}
Interference quantity of X1	72 m^3/d
Interference quantity of X3	10 m^3/d
Interference quantity of X4	0 m^3/d

connectivity analysis, three adjacent wells have good connectivity with it (X1/X3/X4), as shown in Figure 11. When the X2 pressure build-up test was conducted, adjacent wells (X1/X3/X4) were also shut in at the same time, and the locations and parameters of the three interfering wells around the X2 are shown in Table 1. The model proposed in this paper was chosen to match the pressure dynamic curve, as shown in Figure 12. This model was matched with good accuracy, especially for the later stages of the pressure dynamic curve. Table 2 manifests the interpretation results.

6. Conclusion

(1) Aiming at the problem of inclined well test in offshore heavy oil reservoir under multiple well interference, this paper comprehensively considers the permeability stress sensitivity of the reservoir and the threshold pressure gradient of heavy oil and establishes the inclined well test model for dual medium heavy oil reservoir under multiple well interference. And using Green function and superposition principle, the analytical solution under Laplace space is obtained. Finally, the test inclined well pressure dynamic curve is plotted by numerical inversion and with three adjacent wells as an example

(2) The influence law of permeability modulus, threshold pressure gradient, multiwell production, well inclination angle, and well distance for pressure dynamic curve are analyzed in this paper. Under the influence of adjacent wells, the pressure derivative curve of the test inclined well in the later stage warps up and produces multiple "platforms." Through sensitivity analysis, there is a critical well inclination angle of 40° for inclined wells. When the well inclination angle is greater than 40°, vertical radial flow similar to horizontal wells will appear

(3) The new model is applied to the well test interpretation of SZ oilfield in Bohai Bay, and high matching accuracy is obtained. This model not only provides theoretical guidance for multiwell interference well test of the similar type of reservoir but also provides a basis for quantitative characterization of inter well connectivity

Nomenclature

p_f: Fracture system pressure (MPa)
v_{fr}: Radial velocity of fluid in fracture (m/s)
K_{fh}: Fracture horizontal permeability (mD)
v_{fz}: Vertical velocity of fluid in fracture (m/s)
μ: Oil apparent viscosity (mPa·s)
K_{fv}: Fracture vertical permeability
λ_B: Threshold pressure gradient of heavy oil (MPa/m)
p_i: Initial formation pressure (MPa)
r: Distance (m)
ϕ_f: Fracture porosity (dimensionless)
C_{tf}: Fracture compressibility (MPa^{-1})
C_{tm}: Matrix compressibility (MPa^{-1})
V_f: Fracture volume ratio (dimensionless)
K_m: Matrix permeability (mD)
p_m: Matrix system pressure (MPa)
α: Matrix block shape factor (dimensionless)
t: Time (s)
z: Distance (m)
q_{jD}: Dimensionless production of adjacent wells (dimensionless)
r_{jD}: Adjacent well distance (dimensionless)
ξ_D: Perturbation deformation function
s: Laplace factor
ξ_{D0}: Zero order perturbation solution of central inclined well
ξ_{D0j}: Zero order perturbation solution of adjacent well
m: Number of adjacent wells causing interference
η: Wellbore integral factor
θ: Well inclination angle
L: Length of inclined well in reservoir
x_D, y_D, z_D: Coordinate
S: Skin factor.

Data Availability

The data used to support the findings of this study are included within the article.

Conflicts of Interest

The authors declare that they have no conflicts of interest regarding the publication of this paper.

Acknowledgments

This work is supported by the Tianjin Branch of CNOOC Ltd. (YXKY-2018-TJ-04).

References

[1] W. Weilin and A. Hongliang, "Interference pressure analysis model of fractured horizontal well," *Fault-Block Oil & Gas Field*, vol. 26, no. 4, pp. 501–505, 2019.

[2] W. Hongfeng, L. Xiaoping, W. Xiaopei, L. Xiuyu, Z. Songbai, and N. Yanbo, "Application of multi-well interference test technology in exploration and development of Keshen Gasfield," *Petroleum Geology and Recovery Efficiency*, vol. 25, no. 1, pp. 100–105, 2018.

[3] S. Hedong, "Pressure buildup analysis in multi-well systems under interferences from adjacent wells," *Natural Gas Industry*, vol. 36, no. 5, pp. 62–68, 2016.

[4] M. Onur, K. V. Serra, and A. C. Reynolds, "Analysis of pressure-buildup data from a well in a multiwell system," *SPE Formation Evaluation*, vol. 6, no. 1, pp. 101–110, 1991.

[5] T. Marhaendrajana, N. J. Kaczorowski, and T. A. Blasingame, "Analysis and interpretation of well test performance at Arun field," in *The SPE Annual Technical Conference and Exhibition*, Houston, Texas, 1999.

[6] E. S. Adewole, "Interference tests analyses of horizontal and vertical well combinations in a reservoir subject to double-edged water drive," in *The Nigeria Annual International Conference and Exhibition*, Lagos, Nigeria, 2012.

[7] Q. Deng, R.-s. Nie, Y.-l. Jia, X.-l. Wang, Y.-y. Chen, and Y. Xiong, "A new method of pressure buildup analysis for a well in a multiwell reservoir," in *Presented at the SPE North Africa Technical Conference and Exhibition*, Cairo, Egypt, 2015.

[8] Y. He, S. Cheng, J. Qin et al., "Analytical interference testing analysis of multi-segment horizontal well," *Journal of Petroleum Science and Engineering*, vol. 171, pp. 919–927, 2018.

[9] J. Yang, L. I. Qi, F. Chen, Y. Liu, J. Zhang, and D. Gao, "Study on interference testing of fractured-vuggy carbonate reservoirs," *Atlantis Press*, vol. 2017, pp. 510–514, 2017.

[10] A. Kumar, P. Seth, K. Shrivastava, R. Manchanda, and M. M. Sharma, "Integrated analysis of tracer and pressure-interference tests to identify well interference," *SPE Journal*, vol. 25, no. 4, pp. 1623–1635, 2020.

[11] G. Han, Y. Liu, W. Liu, and D. Gao, "Investigation on interference test for wells connected by a large fracture," *Applied Sciences*, vol. 9, no. 1, p. 206, 2019.

[12] C. Shiqing, L. Meng, H. Youwei et al., "A multi-well interference pressure transient analysis method to determine the water source orientation of multi-fractured horizontal well," *Journal of China University of Petroleum(Edition of Natural Science)*, vol. 42, no. 5, pp. 81–88, 2018.

[13] H. Cinco, F. G. Miller, and H. J. Ramey Jr., "Unsteady-state pressure distribution created by a directionally drilled well," *Journal of Petroleum Technology*, vol. 27, no. 11, pp. 1392–1400, 1975.

[14] L. Zhang, M. B. Dusseault, and J. A. Franklin, *Slant Well Production in Media with Permeability Anisotropy*, 1993.

[15] B. R. Sousa, "Slanted well test analysis," *University of Campina(in Portuguese)*, 2012.

[16] H. Li, Q. Zhang, K. Wei, Y. Zeng, and Y. Zhu, "Well test analysis of inclined Wells in the low-permeability composite gas reservoir considering the non-Darcy flow," *Energies*, vol. 15, no. 5, p. 1654, 2022.

[17] Z. Xl, L. Xp, and X. Zhang, "Research on inclined well test model for orthographic fault slabby double porosity reservoir," *Well Testing*, vol. 21, no. 6, 2012.

[18] J. Ruizhong, S. Zeyang, C. Yongzheng, Z. Fulei, Z. Chunguang, and Y. Jianwei, "Dynamical characteristics of inclined well in dual medium low permeability reservoir," *Lithologic Reservoirs*, vol. 30, no. 6, pp. 131–137, 2018.

[19] Y. L. Jia, G. F. Sun, R. S. Nie, J. M. Li, and H. K. Li, "Flow model and well test curves for quadruple-media reservoirs," *Lithologic Reservoirs*, vol. 28, no. 1, pp. 123–127, 2016.

[20] X. Youjie, L. Qiguo, W. Rui, and L. Yicheng, "Pressure transient of fractured horizontal well with complex fracture distribution in composite reservoir," *Lithologic Reservoirs*, vol. 31, no. 5, pp. 161–168, 2019.

[21] C. Zhongliang, W. Nutao, C. Huanghui, J. Tao, and D. Sen, "Well test interpretation about multilayer commingled and inclined well," *Well Testing*, vol. 26, no. 3, pp. 29–32+76, 2017.

[22] G. Li, X. Xin, G. Yu et al., "Effect of asphaltene on threshold pressure gradient of heavy oil in porous media," *Science of Advanced Materials*, vol. 13, no. 2, pp. 273–279, 2021.

[23] D. Zhang, J. Peng, Y. Gu, and Y. Leng, "Experimental study on threshold pressure gradient of heavy oil reservoir," *Xinjiang Petroleum Geology*, vol. 33, no. 2, pp. 201–204, 2012.

[24] H. Stehfest, "Algorithm 368: numerical inversion of Laplace transforms [D5]," *Communications of the ACM*, vol. 13, no. 1, pp. 47–49, 1970.

[25] H. Stehfest, "Remark on algorithm 368: numerical inversion of Laplace transforms," *Communications of the ACM*, vol. 13, no. 10, p. 624, 1970.